Sunquake generation by coronal magnetic restructuring

Russell, A. J. B.; Mooney, M. K.; Leake, J. E.; S Hudson, H. S.

Published in:
Astrophysical Journal

DOI:
10.3847/0004-637X/831/1/42

Publication date:
2016

Document Version
Publisher's PDF, also known as Version of record

The Astrophysical Journal, 831:42 (7pp), 2016 November 1 doi:10.3847/0004-637X/831/1/42

SUNQUAKE GENERATION BY CORONAL MAGNETIC RESTRUCTURING

A. J. B. Russell[1], M. K. Mooney[1,4], J. E. Leake[2], and H. S. Hudson[3,5]
[1] School of Science & Engineering, University of Dundee, Dundee DD1 4HN, UK
[2] Naval Research Laboratory, Washington, DC 20375, USA
[3] Space Sciences Lab, University of California Berkeley, Berkeley, CA 94720, USA
Received 2016 February 25; revised 2016 August 18; accepted 2016 August 18; published 2016 October 26

ABSTRACT

Sunquakes are the surface signatures of acoustic waves in the Sun's interior that are produced by some but not all flares and coronal mass ejections (CMEs). This paper explores a mechanism for sunquake generation by the changes in magnetic field that occur during flares and CMEs, using MHD simulations with a semiempirical FAL-C atmosphere to demonstrate the generation of acoustic waves in the interior in response to changing magnetic tilt in the corona. We find that Alfvén–sound resonance combined with the ponderomotive force produces acoustic waves in the interior with sufficient energy to match sunquake observations when the magnetic field angle changes of the order of 10° in a region where the coronal field strength is a few hundred gauss or more. The most energetic sunquakes are produced when the coronal field is strong, while the variation of magnetic field strength with height and the timescale of the change in tilt are of secondary importance.

Key words: magnetohydrodynamics (MHD) – Sun: atmosphere – Sun: coronal mass ejections (CMEs) – Sun: flares – Sun: helioseismology – Sun: magnetic fields

Supporting material: animation

1. INTRODUCTION

Sunquakes are seismic waves that are observed for some but not all coronal mass ejections (CMEs) and M- and X-class flares. They were first detected on the Sun by Kosovichev & Zharkova (1998) and have since been observed many times, e.g., the events listed by Donea (2011). The associated acoustic wave typically has an energy between 10^{27} and 10^{29} erg and comes from a source with an area of the order of 10 Mm^2, implying energy fluences (time-integrated energy fluxes) of 10^{10}–10^{12} erg cm^{-2}. There are many open questions about sunquakes, most notably the nature of the excitation mechanism or mechanisms. The possibilities currently under consideration can be divided into two categories depending on the force that provides the impulse.

In the first type of mechanism, a pressure wave is generated by impulsive heating (Wolff 1972), which is attributed to thick-target heating of the chromosphere by energetic electrons (Kosovichev & Zharkova 1998) or heating of the photosphere due to backwarming (Lindsey & Donea 2008) or deeply penetrating protons (Zharkova & Zharkov 2007). Wave heating of the photosphere and chromosphere (Russell & Fletcher 2013; Reep & Russell 2016) could also come into this class, as suggested by the observations of Matthews et al. (2015). These explanations seem particularly suited to events where one or more seismic sources are collocated with hard X-ray or white light sources, respectively indicating energetic electrons in the chromosphere or heating of the photosphere. The main theoretical difficulty is that these mechanisms typically invoke the passage of a shock wave into the interior, and radiative losses are expected to strongly damp such shocks, depleting the energy available for the seismic wave. It has, however, been suggested by Lindsey et al. (2014) that a horizontal magnetic field could reduce the radiative losses.

The other driver is Lorentz forces, first suggested by Hudson et al. (2008) and refined by Fisher et al. (2012). Solar flares and CMEs both involve extensive coronal magnetic restructuring, and there is convincing evidence that this changes the photospheric magnetic field. Care is needed when interpreting spectropolarimetric data during a flare since the plasma may not be in local thermal equilibrium. However, photospheric magnetic fields do seem to make rapid irreversible changes during the flare's impulsive phase (Wang et al. 1994; Sudol & Harvey 2005; Petrie & Sudol 2010; Wang & Liu 2010) including abrupt changes to the direction of the magnetic field by several tens of degrees (Petrie 2013), often in association with increased UV emission from the overlying chromosphere (Johnstone et al. 2012). Lorentz forces seem particularly relevant to sunquakes where a magnetic change was seen at a seismic source (e.g., Kumar et al. 2011) or where the locations of seismic sources correspond to footpoints of an erupting flux rope (Zharkov et al. 2011).

This paper presents the first MHD simulations of sunquake generation by Lorentz forces. This new approach to sunquakes yields significant advances in understanding, allowing us to give the first complete account of how magnetic changes launch the acoustic wave, and showing for the first time that a realistic change to the magnetic field in the corona produces an acoustic wave with sufficient energy flux to match sunquake observations.

2. SETUP OF THE SIMULATION

Our study uses an initial model solar atmosphere that extends from the interior to the corona. The semiempirical FAL-C model by Fontenla et al. (2006) provides temperatures for the chromosphere, and we extend the model upwards by joining a 1 MK corona to the top of the FAL-C model with a 150 km thick upper transition region between them, and downwards into the interior using a linear function of height

[4] Also at the School of Physics and Astronomy, University of St. Andrews, St Andrews KY16 9SS, UK.
[5] Present address: SUPA School of Physics and Astronomy, University of Glasgow, Glasgow G12 8QQ, UK.

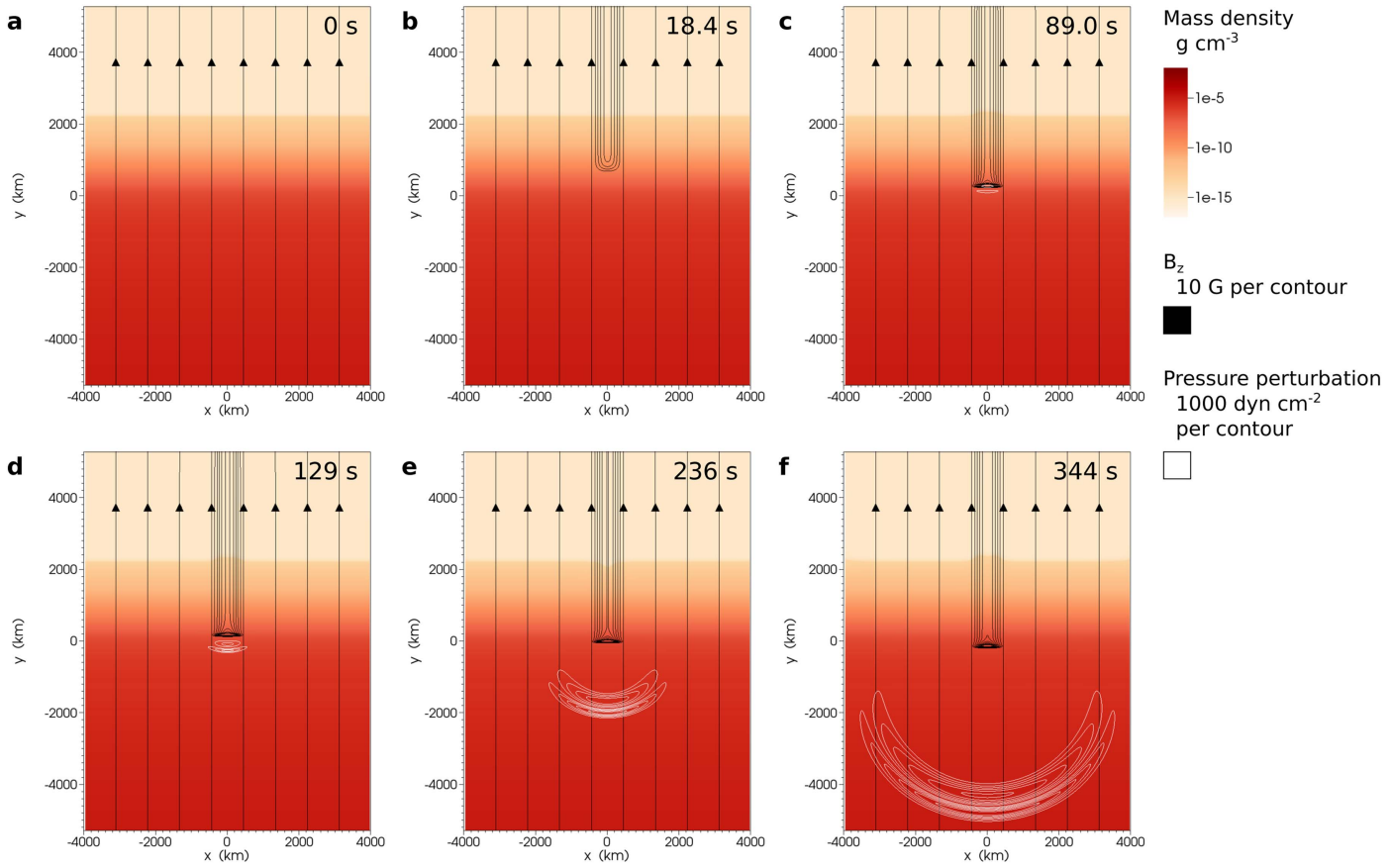

Figure 1. A 2D MHD simulation of acoustic wave generation by changing coronal magnetic field. The logarithmic color scale shows the mass density, field lines show the magnetic field in the x–y plane (initially 250 G), black contours (extending from the top boundary) show B_z, and white contours (the double bow shapes) show the perturbed plasma pressure, $\delta p(\boldsymbol{x}, t) = p(\boldsymbol{x}, t) - p_0(\boldsymbol{x})$. The transition region is the sharp change in density between 2200 and 2400 km, and the sound and Alfvén speeds match at 452 km. The leading pressure perturbation contains increased pressure and the following one has decreased pressure.

(An animation of this figure is available.)

that represents an adiabatic polytrope. Densities are then obtained under an assumption of hydrostatic equilibrium with the photospheric density prescribed by the FAL-C model. The final component is a magnetic field, which is assumed to be vertical in this work since that allows the simplest demonstration of the proposed mechanism. The initial equilibrium is shown in Figure 1(a).

We evolve the model by solving the standard nonlinear MHD equations in 2.5 dimensions using the Lare2d code (the equations and numerical details can be found in Arber et al. 2001). 2.5D means that invariance is assumed in one of the horizontal directions, which we take as the z coordinate, with y the vertical coordinate and x completing the Cartesian triad. The timescales of interest are long compared to the neutral-ion coupling time in the chromosphere (at most a few tens of milliseconds) so a single-fluid description is appropriate. Resistivity, viscosity, thermal conduction, and radiation are neglected for simplicity since they are not essential for sunquake generation to occur, although we caution that these effects may reduce the acoustic energy when they are ultimately included. As discussed in Section 5, future work should examine the impact of radiation on the acoustic waves, while heating due to Cowling resistivity merits investigation in the context of white light emissions at sunquake sources.

The simulation is driven by imposing a velocity in the invariant z direction in the hot corona, which smoothly and continuously displaces the plasma over a chosen timescale, τ_d, thereby tilting the magnetic field. The driving is applied at the top boundary of the simulation, $y = 5286$ km.

3. SUNQUAKE GENERATION

Figure 1 shows a simulation where the coronal magnetic field tilts during a 30 s interval, reaching a maximum inclination of 11° (measured at the top of the domain). The initial field strength is 250 G.

The black contours in Figure 1(b) show B_z at $t = 18.4$ s (measured from the start of the driving). The field change is localized in x with a finite extent imposed by the driver. In the coronal part of the model, the magnetic field is essentially invariant with height—a consequence of the large coronal Alfvén speed (see Figure 2 top). However, a wave front for the change in magnetic field can be identified in the chromosphere as horizontally aligned contours of B_z, and this propagates as an Alfvén wave. As the magnetic change propagates deeper into the atmosphere (Figure 1(c)), the maximum value of B_z in the wave front increases, which we explain as the flux of B_z piling up due to the Alfvén speed being significantly slower ahead of the wave front than behind it. The main time of interest is when the Alfvén wave front crosses the equipartition height, at which the Alfvén speed, $v_A = B/\sqrt{4\pi\rho}$, and the sound speed, $c_s = \sqrt{\gamma kT/m}$, are equal: $y = 452$ km. During this phase an

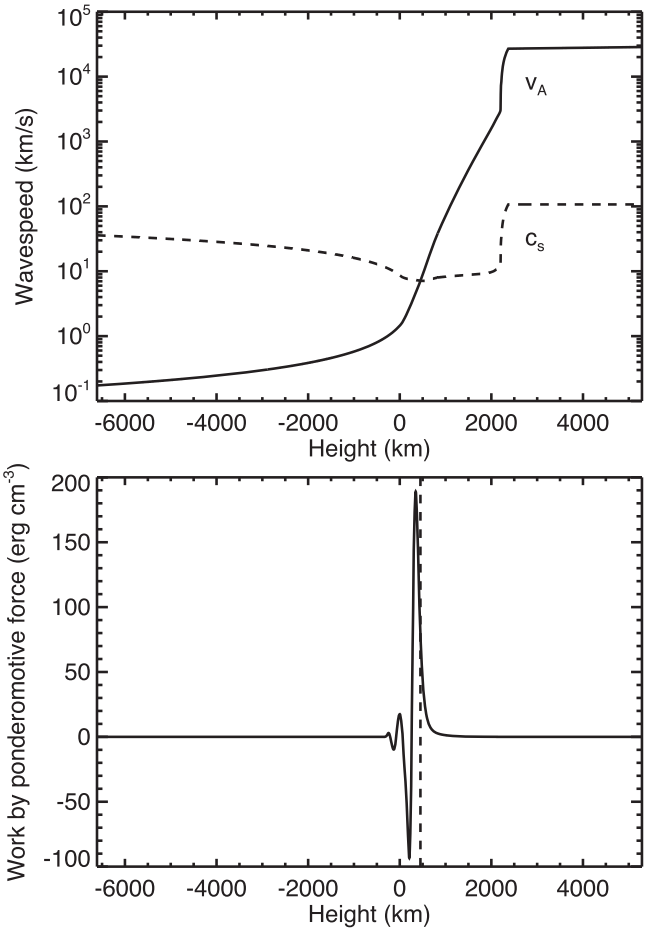

Figure 2. Top: Alfvén speed v_A and sound speed c_s as functions of height for the initial FAL-C equilibrium with $B_0 = 250$ G. The speeds are equal at a height of 452 km. Bottom: work done by the ponderomotive force in a 1D simulation of sunquake generation, showing a resonant peak where the wave speeds match.

acoustic wave is generated, the start of which is visible in Figure 1(c) as an increase in the local pressure slightly ahead of the Alfvénic front followed by a decrease in pressure (white contours). The coupling ends when the resonance is lost, after which the sound wave propagates into the interior and refracts due to the stratified sound speed (panels (d)–(f)). Ultimately, the sound wave will intersect the photosphere, creating the sunquake signature. The Alfvén wave, meanwhile, has slowed to a virtual standstill on the timescale of the simulation, so the change in magnetic field and the associated currents are almost static at later times and do not penetrate far below the photosphere.

We now examine the coupling process. Writing equilibrium quantities with a subscript 0 and perturbed quantities with a delta prefix, we can expand the Lorentz force as

$$\boldsymbol{F}_L = \boldsymbol{J} \times \boldsymbol{B} = \delta\boldsymbol{J} \times \boldsymbol{B}_0 + \delta\boldsymbol{J} \times \delta\boldsymbol{B} \qquad (1)$$

(since our initial equilibrium is current-free we do not include $\boldsymbol{J}_0$ terms). For an Alfvén wave, the leading-order $\delta\boldsymbol{J} \times \boldsymbol{B}_0$ term provides the restoring force: it is in the invariant direction, does not compress the plasma, and therefore does not couple to the sound wave. The $\delta\boldsymbol{J} \times \delta\boldsymbol{B}$ term is the ponderomotive force: it does have a component parallel to the background magnetic field, which allows coupling to the acoustic mode. Ponderomotive effects have been widely studied in the context of other solar phenomena, for example, as a potential source of shocks that heat the chromosphere and form spicules (Hollweg et al. 1982) and as an explanation for the FIP (first ionization potential) effect (Laming 2015). The effects of the ponderomotive force are often small even for nonlinear Alfvén waves because the energy transferred from the Alfvén wave depends on the scalar product of the ponderomotive force and the plasma velocity along the field. Coupling is therefore significant energetically only when the growing sound wave (produced by the coupling) is resonant with the Alfvén wave ($v_A \approx c_s$).

The top panel of Figure 2 shows v_A and c_s in the initial equilibrium. They are equal at 452 km, near which the Alfvén speed decreases rapidly with depth while the sound speed varies only slowly. The bottom panel shows the work done by the ponderomotive force (the time integral of $\boldsymbol{v} \cdot \delta\boldsymbol{J} \times \delta\boldsymbol{B}$ over the entire simulation) at every height for a 1D version of the simulation shown in Figure 1 (with the introduction of the additional assumption of invariance in x). A strong peak is seen at the Alfvén–sound resonance, with the maximum coupling occurring slightly to the lower side of the resonance where v_y is more developed. There is an antiresonance below this where the acoustic wave loses energy because it has become out of phase with the Alfvén wave; hence work is done against the ponderomotive force, not by it. Rapidly diminishing resonances and antiresonances occur lower down. The height-integrated work transfers 2.4×10^9 erg cm^{-2} to the acoustic wave, matching the acoustic energy evaluated in Section 4, with the main contribution coming from the highest resonant peak. We conclude that the ponderomotive force and Alfvén–sound resonance launch the acoustic wave into the interior.

4. ENERGIES

We now investigate whether this mechanism produces acoustic waves with sufficient energy to explain sunquake observations.

The energy of an acoustic wave with low Mach number is closely approximated by the time-integrated enthalpy flux below the coupling region. The enthalpy flux (e.g., Birn et al. 2009) is

$$\boldsymbol{H} = \left(\frac{\gamma}{\gamma-1}\right)p\boldsymbol{v} = \left(\frac{\gamma}{\gamma-1}\right)p_0\,\delta\boldsymbol{v} + \left(\frac{\gamma}{\gamma-1}\right)\delta p\,\delta\boldsymbol{v} \qquad (2)$$

(the $\boldsymbol{v}_0$ terms vanish for our static initial equilibrium). Since the passing of an acoustic wave does not produce a net displacement of the plasma, the linear contribution integrates to zero and we integrate only the second-order term.

Figure 3 (top) shows the time-integrated enthalpy flux at −2000 km for a collection of 1D simulations. Points above the shaded region exceed the lower observable limit of 10^{10} erg cm^{-2} noted in Section 1. The solid curve with crosses (red) shows data for a field strength of 250 G and tilts applied over 30 s, as considered in Section 3. For these parameters, tilts of 20° or more produce acoustic waves that are in principle strong enough to produce observable sunquakes. Figure 3 (bottom) shows the coupling efficiency, defined as the time-integrated enthalpy flux at −2000 km divided by the time-integrated Poynting flux at 2000 km associated with the main Alfvénic front. This figure shows that there are two regimes.

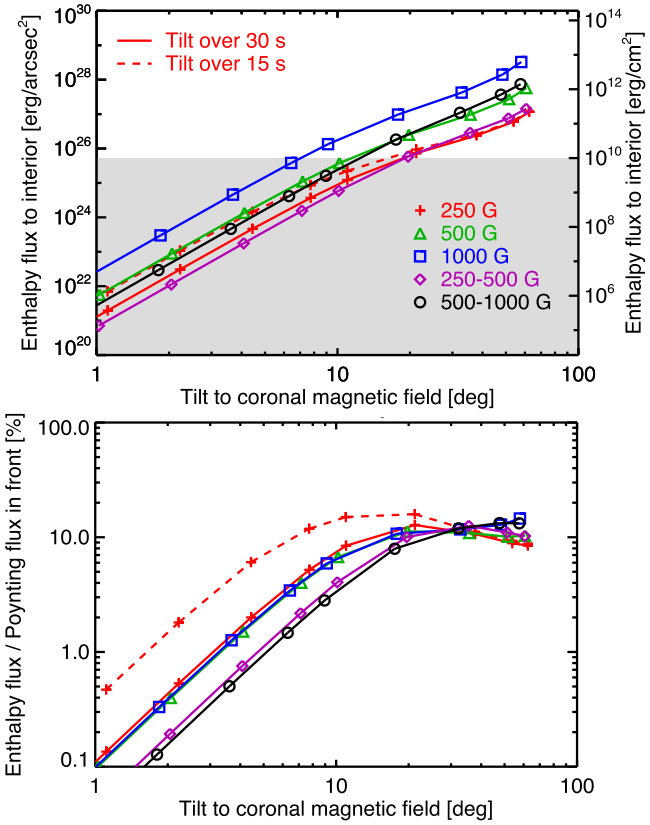

Figure 3. Top: time-integrated enthalpy flux in the acoustic wave (approximately its total energy per source area) for 1D simulations with various magnetic tilts, initial magnetic fields, and driving timescales. Bottom: percentage of the energy in the magnetic front converted to acoustic energy. Where a single magnetic field strength is indicated, the magnetic field was uniform; where a range is given, the field strength was a function of height and the values state the field strength in the corona and at the photosphere.

Writing θ for the change in angle, for tilts up to around 10° the downgoing Alfvénic front evolves as a linear Alfvén wave, the Poynting flux in the front varies as θ^2, and the coupling efficiency varies as θ^2, hence the energy of the acoustic wave varies as θ^4 in the linear regime. For stronger tilts, the downgoing Alfvén wave steepens to form an Alfvénic shock and the conversion efficiency saturates between 10% and 20%. However, the larger Poynting flux associated with stronger driving means that the acoustic energy continues to increase. This strongly nonlinear regime produces the best candidates for observable sunquakes.

The second most important parameter is the magnetic field strength. The triangles (green) in Figure 3 show results for a 500 G field and the squares (blue) show results for 1000 G. For these cases $v_A = c_s$ at 291 km and 117 km respectively. For the parameters we have examined, the conversion efficiency is virtually independent of the field strength; however, larger Poynting flux in the Alfvénic front means that the energy in the acoustic wave increases significantly for stronger magnetic fields (scaling as B_0^2 in the "weak tilt" regime).

Changing the coronal field more rapidly increases the acoustic energy for weak changes in angle but has a negligible effect in the strong regime that appears more relevant to observations. The dashed curve in Figure 3 shows a 15 s driver for a 250 G field. For the weak regime, $\delta \boldsymbol{J}$ in the Alfvénic front is inversely proportional to the vertical scale of the front, which is itself proportional to the duration of the driving; hence quicker drivers produce waves that are more nonlinear, increasing the coupling efficiency. However, once the waves steepen to shocks, the impulse depends on the jump conditions across the magnetic shock, and the acoustic energy becomes independent of the driver timescale.

Finally, we examine 1D simulations where the initial magnetic field strength varies with height, using the scaling of Zweibel & Haber (1983), $B_0 \propto P^{\alpha}$. The diamonds (purple) in Figure 3 show models with 250 G in the corona, rising to 500 G at the photosphere, and the circles (black) have 500 G in the corona and 1000 G at the photosphere. For weak tilts, models with varying $B_0(z)$ produce less acoustic energy than their counterparts with uniform field and the same coronal field strength. This is because the ratio of Alfvén speeds between the coupling height and corona is less extreme, giving less pile-up of magnetic flux in the magnetic front, smaller $\delta \boldsymbol{B}$ and $\delta \boldsymbol{J}$, smaller ponderomotive force, and ultimately less efficient coupling. This effect is lost for large tilts. In fact, in the strong regime, height variation of $B(z)$ assists generation of the acoustic wave because the Alfvénic shock dissipates less energy while propagating to the coupling height.

5. DISCUSSION

The MHD simulations in this paper show that changes in magnetic field direction are most acoustically active when the direction of a strong magnetic field changes by tens of degrees. The X2.2 flare on 2011 February 15 studied by Petrie (2013) changed the photospheric magnetic angle by several tens of degrees, so while such changes are large, they have an observational basis for large flares.

The energy of the modeled acoustic wave becomes independent of the driving timescale when the magnetic change is large enough and fast enough that the Alfvénic front shocks before reaching the Alfvén–sound resonance, while for linear dynamics rapid magnetic changes are more effective at producing acoustic waves than gradual changes. Sudol & Harvey (2005) fitted time series of GONG magnetogram data for 15 X-class flares, and one third of the irreversible magnetic changes they identified had durations of less than 1 minute, which is the cadence of their observations. We conclude that the driver durations used in our simulations (30 and 15 s) are plausible for the most dynamic locations. Considering longer timescales, half of the changes studied by Sudol & Harvey (2005) had a duration of less than 1.5 minutes and three-quarters had duration less than 10 minutes, although durations as long as several tens of minutes were also found. Therefore it may be relevant to some events that the acoustic flux does depend on driving timescale when sufficiently slow, even for large changes to the magnetic field.

The observation that would most naturally support our model, or rule it out for a given event by an unambiguous absence, is a suitable magnetic change near the acoustic source, consistent with the time at which the acoustic wave is launched. The idea of such a test is not new, but our results justify some remarks.

Figure 1 indicates that the acoustic source should be horizontally aligned with the change in magnetic field, consistent with the thesis of Martínez-Oliveros & Donea (2009) and Alvarado-Gómez et al. (2012) that these regions should be in close proximity. A small offset is expected when

the magnetic field is inclined and the radiation providing the magnetic measurements comes from a different height to the acoustic source. If chromospheric magnetic data are available, then a change there should precede the photospheric change by the Alfvén travel time (as a guideline, several tens of seconds), which may help to distinguish magnetic changes due to coronal restructuring from other causes such as flux emergence. We caution that magnetic changes may not show up in the line-of-sight magnetic field—the vertical magnetic field does not change at all in our simulations—or they may be missed in unresolved observations, e.g., if just a localized change in the magnetic twist. Thus, to be conclusive, such a test requires high-resolution vector measurements and careful treatment of the possibility of spatially unresolved magnetic changes.

Continuing this theme, an interesting feature of our simulations is that the magnetic field undergoes a reversible change in addition to the irreversible change, producing a combined evolution of magnetic field similar to the ones plotted for the seismic sources observed by Martínez-Oliveros & Donea (2009) and Alvarado-Gómez et al. (2012) (Figure 3 in each paper). In our simulations, the reversible change is physical, the product of the flux of B_z piling up in the Alfvén wave front when the Alfvén speed is significantly lower ahead of the wave front than behind it. There are good reasons to be cautious about short-lived features in magnetograms during flares in case they are spurious, which has led to sunquake generation by magnetic effects being assessed based on the irreversible component only (e.g., Alvarado-Gómez et al. 2012). However, our study indicates that the reversible part of magnetic signatures may actually correspond to a real reversible magnetic field perturbation. Consideration should therefore be given to the role of this reversible component in the energetics of sunquake excitation and whether it is possible that Lorentz drivers could be significant in events where they previously appeared to have been ruled out.

It should be emphasized as well that our simulations generate the acoustic wave by resonant coupling, and the connection between changes in magnetic field and acoustic waves is therefore more nuanced than a simple association between seismic sources and large changes in magnetic field or Lorentz force. A given magnetic change may succeed in producing or fail to produce a detectable sunquake depending on properties such as the degree of nonlinearity, the sound and Alfvén speed profiles, and the timescale. These effects were not apparent from early theoretical works on this topic (Hudson et al. 2008; Fisher et al. 2012), and it is our application of MHD theory that allows us to identify them now. Future modeling may establish further properties that favor sunquake generation at particular locations; for example, the relative heights of Alfvén–sound resonance and the transition between optically thin and thick radiation may be significant when radiative damping is included.

The possibility of resonant coupling is also relevant to constraints that do not rely on observed field changes. A study by Judge et al. (2014) of the main acoustic source in the X1 flare on 2014 March 29 reached an interesting set of conclusions, namely, that the sunquake power was at least two times greater than the downward enthalpy flux obtained using the Si I line core, Poynting fluxes estimated using photospheric densities were only marginally sufficient for nonlinear perturbations, and several other forms of energy transport were ruled out. How could the sunquake have been excited when it appears that no single transport mechanism operated through the full atmosphere? The Si I core typically forms at a height between 200 and 500 km in 1D models (Judge et al. 2014), and we would expect this to be above the $v_A = c_s$ surface for the reported field strength of 800 G. Thus, if our mechanism were applied, the downward energy transport at the heights of the Si I core would predominantly be as Poynting flux, which is very capable at these altitudes since the density is almost an order of magnitude lower than at the photosphere. As energy approaches depths where Poynting flux cannot carry the required power, a portion is converted to an enthalpy flux to form the sunquake, but only below the altitudes sampled by the Si I line. Conversion of energy fluxes therefore resolves the apparent paradox. Combining MHD simulations and observations using techniques such as forward modeling should be a useful future partnership in this area.

It is pertinent at this point that our Figure 3 (bottom) indicates a new and stronger constraint since at most 10% to 20% of the integrated Poynting flux into the acoustic kernel is converted to sunquake energy. Interestingly, this percentage of the Poynting flux for a nonlinear magnetic front at the Si I core height agrees well with the acoustic power per unit area for the 2014 March 29 sunquake. However, one should not read too much into this without supporting evidence of actual magnetic changes, which are currently unclear for this event (flux emergence at the time of the flare and near the acoustic source complicates interpretation of magnetic changes). We also point out that since sunquake energy typically represents about 0.01%–0.1% of the total flare energy (Donea 2011), one or more of the following must be true: the Poynting-flux energy that acoustically active magnetic changes direct into the acoustic kernel is of the order of 0.1%–1% of the total flare energy (this does not include higher frequency waves of the sort considered by Reep & Russell 2016), or the conversion efficiency actually attained is less than the maximum identified in this study, for example, due to dissipative processes that were not included in our simulations.

Future MHD modeling will add radiation, thermal conduction, and resistivity, all of which may reduce the acoustic energy that ultimately enters the interior. Radiation is particularly important because it modifies and damps acoustic waves in the lower atmosphere (Fisher et al. 1985) and is therefore regarded as an obstacle to all sunquake mechanisms (Fisher et al. 2012; Lindsey et al. 2014). The Alfvén–sound resonance mechanism described in this paper appears to have an advantage over particle beams in this regard because the Alfvén–sound resonance can potentially occur below the layers where acoustic waves are most strongly damped by radiation. This applies primarily in regions of strong magnetic field strength such as sunspot penumbra, which is where sunquake sources are almost exclusively observed. Future work should test this as a priority. We also note that the relatively large perpendicular resistivity in the chromosphere (Russell & Fletcher 2013; Leake et al. 2014) may dissipate some of the energy in the Alfvénic front before the acoustic wave is generated, thereby reducing the acoustic energy, and it remains to be shown whether or not these losses are significant.

Another goal for future modeling is to address more general initial equilibria. For example, sunquake sources are typically located in sunspot penumbra where the magnetic field is inclined from the outset, whereas we used an initially vertical magnetic field in this paper to simplify presentation of the

theory and simulations. Similarly, the work presented did not include the geometrical effects of magnetic field convergence, which may alter $\delta B/B_0$ in the wave front and hence the efficiency of the resonant coupling. Some magnetic field strengths and profiles may also move the $v_A = c_s$ resonance below the photosphere, where the gradient of v_A/c_s at the resonance becomes gentler (Figure 2), which could in principle increase the efficiency of the resonant coupling by allowing it to occur over a larger interval. Consideration of non-potential magnetic fields (for which $\boldsymbol{J}_0$ is non-zero) and non-static equilibria with background flows (such as the Evershed flow) would also be worthwhile.

Simulation studies based on localized regions are clearly valuable by themselves, but future consideration should be given to the wider magnetic context of the flare as well. One motivation for this is that the decrease in magnetic energy believed to power flares is a global phenomenon. In the simulations presented here, localized shearing of the magnetic field by the applied driving increases the magnetic energy in the simulation domain by making the magnetic field more inclined. This is known to occur in localized regions of the photosphere, with the local increases in magnetic energy more than balanced by decreases elsewhere in the active region (Fletcher et al. 2011). A local reduction in the field inclination should also produce acoustic waves by the resonant coupling mechanism, as should changes to the magnetic azimuth, but some important physical differences mean that these scenarios should be explored in their own right. Insights into the global pattern of magnetic changes in an active region during flares will be able to inform MHD studies of sunquake generation near particular features such as the polarity inversion line or hooks on flare ribbons. At the more ambitious end, since seismic sources of sunquakes have been observed that are coincident with the end points of an erupting flux rope (Zharkov et al. 2011), it would be very interesting to explore this association by coupling a global MHD simulation of an erupting flux rope (similar, for instance, to Aulanier et al. 2010) to a chromospheric model capable of capturing the resonant excitation. Such an undertaking would be comparable in scale to present-day simulations of flux emergence and is therefore feasible with appropriate computing resources.

Alfvén wave fronts are only one method by which Lorentz forces may generate acoustic waves in the interior. Another possibility is the transmission and mode conversion of magnetoacoustic waves originating in the corona, as considered analytically by Hansen et al. (2016). MHD simulations of the type presented here can readily be adapted to the scenario they propose. Waveguided fast waves (Russell & Stackhouse 2013) and modes of the coronal structures (e.g., kink and sausage waves) would be interesting to consider in that context.

Finally, we point out two additional interesting features of our simulations. The first is that the change in magnetic field excites an oscillation that displaces the transition region with a period of 200 s, or approximately 3 minutes. This is evident in Figure 1 and can be seen clearly in the online animation. The simulated vertical velocity reaches up to a few tens of kilometers per second for large magnetic changes; for comparison, *IRIS* (De Pontieu et al. 2014) has a velocity resolution of $1\,\mathrm{km\,s^{-1}}$. The other feature we highlight is the perpendicular current just below the photosphere at the end of our simulations (Figure 1(f)). Coronal magnetic changes alter the coronal current system (our driver creates a pair of upward and downward field-aligned currents), and since the current in the deep interior is unchanged, current continuity requires a new perpendicular current somewhere between these domains. The Alfvénic front naturally provides the required current closure (Wheatland & Melrose 1994), even when frozen by the vanishing Alfvén speed. The relatively large perpendicular resistivity at photospheric heights (Russell & Fletcher 2013; Leake et al. 2014) suggests that the perpendicular current should heat the photosphere, potentially enhancing the optical emission where the tilt has changed—a possibility that deserves investigation.

6. CONCLUSIONS

1. MHD simulations establish that changes to the coronal magnetic field excite acoustic waves in the solar interior with energy fluences matching or exceeding typical values for observed sunquakes.
2. The acoustic wave is produced at the Alfvén–sound resonance in the lower atmosphere by the ponderomotive force in the Alfvénic front associated with the magnetic change.
3. The most acoustically active changes to magnetic field direction are changes of tens of degrees on magnetic fields of hundreds or thousands of gauss.

This work came out of the International Space Science Institute (Switzerland) Team 326 "Magnetic Waves in Solar Flares" led by A.J.B.R. and Lyndsay Fletcher (http://www.issibern.ch/teams/flarewaves). We thank ISSI for supporting the activity and the team members for useful discussions. We acknowledge grant ST/K000993/1 from STFC to the University of Dundee (A.J.B.R.) and summer student support from the School of Science & Engineering (M.K.M.). J.E.L. was funded by NASA's Living With a Star Program and the Chief of Naval Research. The 2D simulation was run on the St Andrews MHD cluster (supported by STFC's Dirac programme) and analyzed using VisIt (supported by the U.S. Department of Energy). We thank an anonymous referee for highly constructive comments.

REFERENCES

Alvarado-Gómez, J. D., Buitrago-Casas, J. C., Martínez-Oliveros, J. C., et al. 2012, SoPh, 280, 335
Arber, T. D., Longbottom, A. W., Gerrard, C. L., & Milne, A. M. 2001, JCoPh, 171, 151
Aulanier, G., Török, T., Démoulin, P., & DeLuca, E. E. 2010, ApJ, 708, 314
Birn, J., Fletcher, L., Hesse, M., & Neukirch, T. 2009, ApJ, 695, 1151
De Pontieu, B., Title, A. M., Lemen, J. R., et al. 2014, SoPh, 289, 2733
Donea, A. 2011, SSRv, 158, 451
Fisher, G. H., Bercik, D. J., Welsch, B. T., & Hudson, H. S. 2012, SoPh, 277, 59
Fisher, G. H., Canfield, R. C., & McClymont, A. N. 1985, ApJ, 289, 434
Fletcher, L., Dennis, B. R., Hudson, H. S., et al. 2011, SSRv, 159, 19
Fontenla, J. M., Avrett, E., Thuillier, G., & Harder, J. 2006, ApJ, 639, 441
Hansen, S. C., Cally, P. S., & Donea, A.-C. 2016, MNRAS, 456, 1826
Hollweg, J. V., Jackson, S., & Galloway, D. 1982, SoPh, 75, 35
Hudson, H. S., Fisher, G. H., & Welsch, B. T. 2008, in ASP Conf. Ser. 383, Subsurface and Atmospheric Influences on Solar Activity, ed. R. Howe et al. (San Francisco, CA: ASP), 221
Johnstone, B. M., Petrie, G. J. D., & Sudol, J. J. 2012, ApJ, 760, 29
Judge, P. G., Kleint, L., Donea, A., Sainz Dalda, A., & Fletcher, L. 2014, ApJ, 796, 85
Kosovichev, A. G., & Zharkova, V. V. 1998, Natur, 393, 317
Kumar, B., Venkatakrishnan, P., Mathur, S., Tiwari, S. K., & García, R. A. 2011, ApJ, 743, 29
Laming, J. M. 2015, LRSP, 12, 2

Leake, J. E., DeVore, C. R., Thayer, J. P., et al. 2014, SSRv, 184, 107
Lindsey, C., & Donea, A.-C. 2008, SoPh, 251, 627
Lindsey, C., Donea, A.-C., Martínez Oliveros, J. C., & Hudson, H. S. 2014, SoPh, 289, 1457
Martínez-Oliveros, J. C., & Donea, A.-C. 2009, MNRAS, 395, L39
Matthews, S. A., Harra, L. K., Zharkov, S., & Green, L. M. 2015, ApJ, 812, 35
Petrie, G. J. D. 2013, SoPh, 287, 415
Petrie, G. J. D., & Sudol, J. J. 2010, ApJ, 724, 1218
Reep, J. W., & Russell, A. J. B. 2016, ApJL, 818, L20
Russell, A. J. B., & Fletcher, L. 2013, ApJ, 765, 81
Russell, A. J. B., & Stackhouse, D. J. 2013, A&A, 558, A76
Sudol, J. J., & Harvey, J. W. 2005, ApJ, 635, 647
Wang, H., Ewell, M. W., Jr., Zirin, H., & Ai, G. 1994, ApJ, 424, 436
Wang, H., & Liu, C. 2010, ApJL, 716, L195
Wheatland, M. S., & Melrose, D. B. 1994, AuJPh, 47, 361
Wolff, C. L. 1972, ApJ, 176, 833
Zharkov, S., Green, L. M., Matthews, S. A., & Zharkova, V. V. 2011, ApJL, 741, L35
Zharkova, V. V., & Zharkov, S. I. 2007, ApJ, 664, 573
Zweibel, E. G., & Haber, D. A. 1983, ApJ, 264, 648